

Double pion photoproduction off ^{40}Ca

F. Bloch¹, J. Ahrens², J.R.M. Annand³, R. Beck², L.S. Fog³, D. Hornidge², S. Janssen⁴, M. Kotulla^{1 a}, B. Krusche¹, J.C. McGeorge³, I.J.D. MacGregor³, J.G. Messchendorp^{4 b}, V. Metag⁴, R. Novotny⁴, R.O. Owens³, M. Pfeiffer⁴, M. Rost², R. Sanderson³, S. Schadmand^{4 c}, A. Thomas², D.P. Watts³

¹ Department of Physics and Astronomy, University of Basel, Ch-4056 Basel, Switzerland

² Institut für Kernphysik, Johannes-Gutenberg-Universität Mainz, D-55099 Mainz, Germany

³ Department of Physics and Astronomy, University of Glasgow, Glasgow G12 8QQ, UK

⁴ II. Physikalisches Institut, Universität Giessen, D-35392 Giessen, Germany

Received: date / Revised version: date

Abstract. The photoproduction of $\pi^0\pi^0$ and $\pi^0\pi^\pm$ pairs off ^{40}Ca has been investigated with the TAPS detector using the Glasgow photon tagging spectrometer at the Mainz MAMI accelerator. Data have been taken for incident photon energies in the energy range from 200 - 820 MeV. Total cross sections have been extracted from threshold up to the maximum photon energy and invariant mass distributions of the pion pairs have been obtained for incident photon energies between 400 - 500 MeV and 500 - 550 MeV. The double π^0 invariant mass distributions show some relative enhancement with respect to the mixed charge channel at small invariant masses. The effects are smaller than previously observed for lead nuclei and the distributions do not significantly deviate from carbon data. The data are in good agreement with the results of recent calculations in the framework of the BUU model, with careful treatment of final state interaction effects but without an explicit in-medium modification of scalar, iso-scalar pion pairs. This means that for Ca most of the experimentally observed effect can be explained by final state interactions. Only at low incident photon energies there is still a small low mass enhancement of the double π^0 data over the BUU results.

PACS. 13.60.Le meson production – 25.20.Lj photoproduction reactions

1 Introduction

In-medium properties of hadrons are a hotly debated topic since they are closely related to the properties of low-energy, non-perturbative QCD. QCD at high energies or short scales ($r < 0.1\text{fm}$) is well explored by perturbative methods. However, at larger distances the perturbative picture breaks down and at scales between 0.1 fm and 1 fm the full complexity of the interaction manifests itself in the many body structure of hadrons composed of valence quarks, sea quarks, and gluons. Chiral symmetry is at the very heart of the theory. In the limit of vanishing current quark masses the QCD Lagrangian is invariant under chiral rotations, right and left handedness of quarks is conserved and right and left handed fields can be treated independently. The explicit breaking of the symmetry due to finite u,d current quark masses (5-15 MeV) is small. How-

ever, it is well known that spontaneous breaking occurs since the ground state, the QCD vacuum, has only part of the symmetry. This is connected to a non-zero expectation value of scalar $q\bar{q}$ pairs in the vacuum, the chiral condensate. The symmetry breaking is clearly reflected in the hadron spectrum. Without it, hadrons should appear as mass degenerate parity doublets, which is neither true for baryons nor for mesons. The first $J^\pi=1/2^-$ excited state in the baryon spectrum, the $S_{11}(1535)$ lies much above the $J^\pi=1/2^+$ nucleon ground state. The lowest lying $J^\pi=1^-$ vector meson, the ρ , has a smaller mass than the $J^\pi=1^+$ a_1 , and the $J^\pi=0^-$ pion (the Goldstone boson of chiral symmetry), is much lighter than its chiral partner, the $J^\pi=0^+$ σ -meson.

However, model calculations (see e.g. [1]) indicate a significant temperature and density dependence of the chiral condensate which is connected with a partial restoration of chiral symmetry at high temperature and/or large densities. An observable consequence is a density and temperature dependence of hadron masses. These effects will be most pronounced for the high temperature/density conditions probed in heavy ion reactions, but they should be already significant at zero temperature and normal nuclear density as probed by pion and photon beams. In-medium

Send offprint requests to: Bernd.Krusche@unibas.ch

^a Present address: II. Physikalisches Institut, Universität Giessen, D-35392 Giessen, Germany

^b Present address: Kernfysisch Versneller Instituut (KVI), Groningen, The Netherlands

^c Present address: Institut für Kernphysik, Forschungszentrum Jülich, D-52425 Jülich, Germany

modifications of vector mesons have been searched for via the spectroscopy of di-lepton pairs emitted in heavy ion reactions by the CERES experiment [2,3] and more recently the NA60 collaboration [4], which reported a strong broadening of the in-medium spectral function of the ρ -meson. A signature for in-medium modifications of ρ and ω mesons was also reported from the E325 experiment in 12 GeV p+A reactions at KEK [5]. An in-medium mass shift of the ω meson has been found in photon induced ω -production from heavy nuclei [6]. Due to their coupling to vector mesons, nucleon resonances should also be modified in the nuclear medium. Self-consistent calculations of the respective spectral functions [7] predict in particular significant effects for the $D_{13}(1520)$ resonance, which have also been searched for in photon induced meson production reactions [8,9,10,11], however so far without conclusive results. As discussed in detail by Lehr and Mosel [12], part of the problem is, that due to the averaging over the nuclear volume, a possible broadening of the resonance can be only observed via decay channels which cause the broadening, but not in other exclusive reactions.

A particularly interesting case is the mass-split between the $J^\pi=0^-$ pion and the $J^\pi=0^+$ σ -meson. The naive assumption that the two masses should become degenerate in the chiral limit is supported by model calculations. A typical result is the density dependence of the mass calculated in the Nambu-Jona-Lasino model by Bernard, Meißner and Zahed [13]. The σ -mass drops significantly as function of nuclear density. Compared to the vacuum the predicted effect is already large for normal nuclear matter density ρ_0 at which the pion mass stays still stable. The nature of the σ meson itself has been controversially discussed in the literature. The review of particle properties [14] lists as σ the $f_0(600)$ with a mass range from 400 - 1200 MeV and a full width between 600 MeV and 1000 MeV. Recently, Caprini, Colangelo and Leutwyler [15] have derived precise predictions for mass and width from dispersion relations. In some approaches it is treated as a pure $q\bar{q}$ (quasi)bound state [13,16,17], in other approaches as a correlated $\pi\pi$ pair in a $I=0, J^\pi=0^+$ state [18,19,20]. But in any case a strong coupling to scalar, iso-scalar pion pairs is predicted. As a consequence, the different model approaches agree in so far, as they predict a significant in-medium modification of the invariant mass distribution of such pion pairs. This is either due to the in-medium spectral function of the σ meson [16] or the in-medium modification of the pion-pion interaction [19] due to the coupling to nucleon - hole, Δ - hole and N^* - hole states. In any case the predicted net effect is a downward shift of the strength in the invariant mass distributions of scalar, iso-scalar pion pairs in nuclear matter.

First experimental evidence for this effect has been reported by the CHAOS collaboration from the measurement of pion induced double pion production reactions [21,22,23,24,25]. The main finding was a build-up of strength with rising mass number at low invariant masses for the $\pi^+\pi^-$ final state, but not for the $\pi^+\pi^+$ channel where the σ as neutral particle cannot contribute. A similar effect was found by the Crystal Ball collaboration at BNL.

They observed a low-mass enhancement of strength for heavy nuclei in the $\pi^- A \rightarrow A\pi^0\pi^0$ reaction [26].

Pion induced reactions have the disadvantage that the signal is diluted by final (FSI) and initial (ISI) state interaction of the pions, so that effectively only the low-density surface zone of the nuclei is probed. Pions can be produced in the entire volume of the nuclei by photon induced reactions, although their FSI also suppresses the contributions from the deep interior of the nuclei. The FSI can be minimized by the use of low incident photon energies, giving rise to low-energy pions which have much larger mean free paths than pions that can excite the Δ -resonance [9]. Photoproduction of the different charge states of pions from the free proton and the quasifree neutron has been previously studied in detail with the DAPHNE [27,28,30,31,32] and TAPS detectors [33,34,35,36,37,38] at MAMI in Mainz from threshold to the second resonance region and for the $\pi^0\pi^0$ channel also at higher incident photon energies at GRAAL in Grenoble [39] (see [40] for an overview).

First results from a measurement of double π^0 and $\pi^0\pi^\pm$ photoproduction off carbon and lead have been reported in [41]. A shift of the strength to lower invariant masses was found for the heavier nucleus for the $\pi^0\pi^0$ channel but not for the mixed charge channel. In the present paper, experimental details and the results of an additional measurement of double pion photoproduction off calcium nuclei are presented and compared to model calculations.

2 Experimental setup

The experimental setup was identical to the measurement of double pion photoproduction off carbon and lead nuclei reported in [41]. Some further experimental details have been discussed in [9].

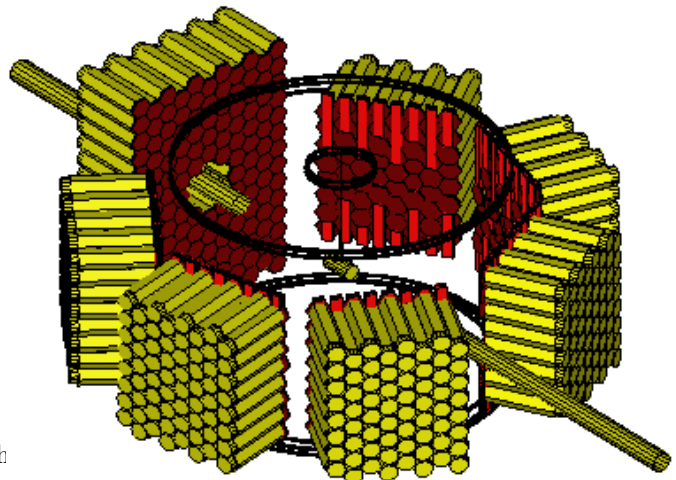


Fig. 1. Setup of the TAPS detector at the Mainz MAMI accelerator. The beam entered the target chamber from the lower right edge.

Quasi-monochromatic photons were produced with the Glasgow tagged photon facility [42] at the Mainz MAMI accelerator [43]. The experiment covered the photon energy range from 200 - 800 MeV with an energy resolution of approximately 2 MeV per tagger channel. The target was a 10 mm long cylinder of calcium with 50 mm diameter and the beam-spot size at the target position was approximately 30 mm. The reaction products from the target were detected with the electromagnetic calorimeter TAPS [44,45]. This detector consists of 510 hexagonally shaped BaF_2 crystals of 25 cm length with an inner diameter of 5.9 cm. As shown in fig. 1 they were arranged in six blocks of 64 modules and a larger forward wall of 138 modules. The blocks were arranged in one plane around the target at a distance of 55 cm from the target center and at polar angles of $\pm 54^\circ$, $\pm 103^\circ$, and $\pm 153^\circ$, while the forward wall was placed 60 cm away from the target center at 0° and the photon beam passed through a hole in the center of the forward wall. Each detector module is equipped with an individual plastic veto detector, read out by a separate photomultiplier. The setup covered approximately 37 % of the full solid angle.

3 Data analysis

The first step of the analysis for both final states - $\pi^0\pi^0$ and $\pi^0\pi^\pm$ - requires the identification of photons. This was done with the help of the veto detectors, a time-of-flight analysis (time resolution: 550 ps FWHM), and a pulse shape analysis of the signals from the BaF_2 scintillator. The latter is based on the two different components of the scintillation light from BaF_2 crystal, which have very different decay times. The relative intensity of the fast component depends on the ionization density produced by the incident particle, in particular it is suppressed for nucleons in comparison to photons. This feature was exploited by integrating the output signals over a short gate (40 ns) and a long gate (2 μs). Both signals E_s (short gate) and E_w (wide gate) were calibrated for photons so that in an E_s -versus- E_w plot photons are lying on the 45° line. This is shown in the left hand side of fig. 2. For the discrimination between photons and nucleons a representation in polar coordinates (see right hand side of fig. 2)

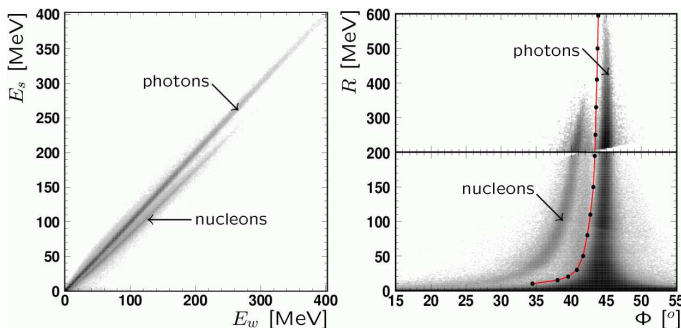


Fig. 2. Pulse shape analysis. Left hand side: plot of E_s versus E_w . Right hand side: plot in polar coordinates.

is more efficient. The respective coordinates are the radius $R = \sqrt{E_s^2 + E_w^2}$ and the angle $\Phi = \arctan(E_s/E_w)$. The combination of the different discrimination methods provides a clean sample of photons.

For the investigation of the $\pi^0\pi^0$ final state events with four photons were selected. The invariant masses of all possible combinations of the four photons into two pairs were calculated and the ‘best’ combination was chosen via a χ^2 analysis which minimizes

$$\chi^2 = \frac{(m_{\gamma_i, \gamma_j} - m_\pi)^2}{\Delta m_{\gamma_i, \gamma_j}} + \frac{(m_{\gamma_k, \gamma_l} - m_\pi)^2}{\Delta m_{\gamma_k, \gamma_l}} \quad (1)$$

with $1 \leq i \neq j \neq k \neq l \leq 4$, where m_π is the pion mass, the $m_{\gamma, \gamma}$ are the invariant masses of the photon pairs, and the $\Delta m_{\gamma, \gamma}$ are the associated uncertainties. A two-dimensional representation of the invariant masses of these pion pairs is shown in fig. 3. Events with both invariant masses in the range 100 - 150 MeV were selected.

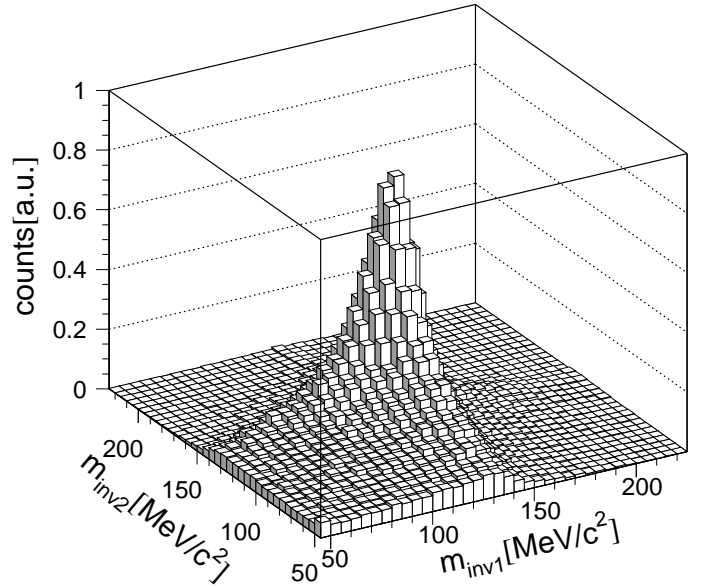


Fig. 3. Invariant mass of photon pair 1 versus invariant mass of photon pair 2 for events with four detected photons.

At incident photon energies below the η production threshold this analysis results in a practically background-free data sample for the $\pi^0\pi^0$ final state. Above the η threshold background arises from $\eta \rightarrow \pi^0\pi^0\pi^0$ decays, where the decay photons from one π^0 escape detection due to the limited solid angle of the calorimeter. This background can be partly suppressed by a missing mass analysis. It is assumed that the reaction occurs quasi-free off one participant nucleon. The initial momentum of this bound nucleon is neglected. The mass of the missing particle - the participant nucleon - is then determined by the energy of the incident photon E_b and the four-vectors of the four decay photons apart from the effects of Fermi motion, which broaden the missing mass distributions. The

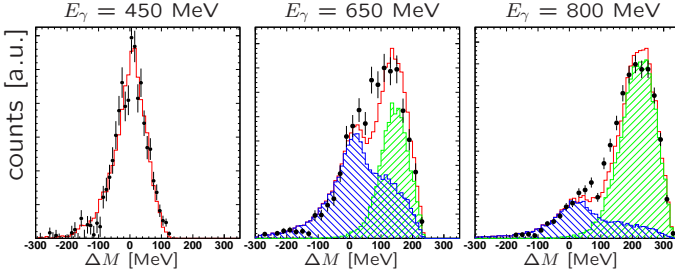


Fig. 4. Missing mass spectra for double π^0 photoproduction from Ca. Left side: incident photon energy range 400 - 500 MeV (below η threshold), middle and right hand side above η threshold: E_γ around 650 and 800 MeV, respectively. Closed circles: experiment, shaded histograms: simulation of $2\pi^0$ photoproduction (around zero) and η photoproduction, solid histograms: sum of both.

missing mass ΔM is given by:

$$\Delta M = \sqrt{(E_b + m_N - \sum_{i=1}^4 E_{\gamma_i})^2 - (\mathbf{P}_b - \sum_{i=1}^4 \mathbf{P}_{\gamma_i})^2 - m_N^2} \quad (2)$$

where E_{γ_i} and \mathbf{P}_{γ_i} are energies and momenta of the decay photons and m_N is the nucleon mass. The resulting distributions are shown in fig. 4 for energies below and above the η production threshold. They are compared to Monte Carlo simulations which take into account Fermi motion, a simple approximation of final state interaction (FSI) of the mesons, and the detector acceptance and detection efficiency. The simulation of the detector response was based on the GEANT3 package [46]. At incident photon energies below the η threshold the data agree very well with the results of the simulation and no indication of background is visible. The background from η decays is prominent at higher incident photon energies, but the data can still be reproduced by a superposition of simulated double π^0 and $\eta \rightarrow \pi^0\pi^0\pi^0$ events. Due to the large broadening of the missing mass structures by Fermi motion and FSI (responsible for the shoulders of the double π distributions) a clear separation of the two reaction channels is not possible. However, the cross section for η photoproduction is simultaneously measured via their $\eta \rightarrow \gamma\gamma$ decay. With this cross section and the known decay branching ratios it is possible to simulate the contribution of $\eta \rightarrow \pi^0\pi^0\pi^0$ decays to the analysis of double π^0 decays. If this is done without any cut on missing mass, the result becomes independent of the simulated shapes of the distributions, but the statistical quality suffers since at high incident photon energies the η background contribution is large. Therefore as a compromise only events with missing mass between -100 and 100 MeV were selected, so that the background contribution from the η decays did not exceed 20 %.

The analysis of the $\pi^0\pi^\pm$ final state is more difficult. In the first step events with two photons and the invariant mass of the photon pair (see fig. 7, left hand side) between 100 and 150 MeV were selected. In the second step an additional particle was required. Candidates for charged pions were then selected by a time-of-flight ver-

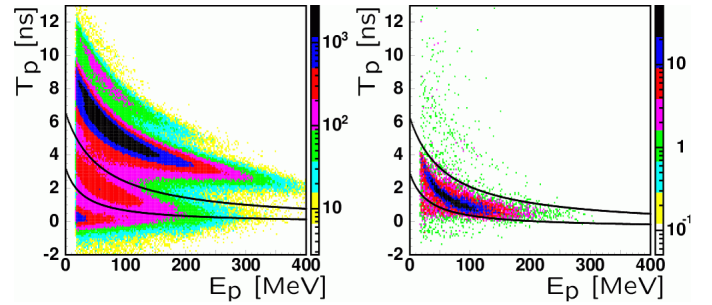
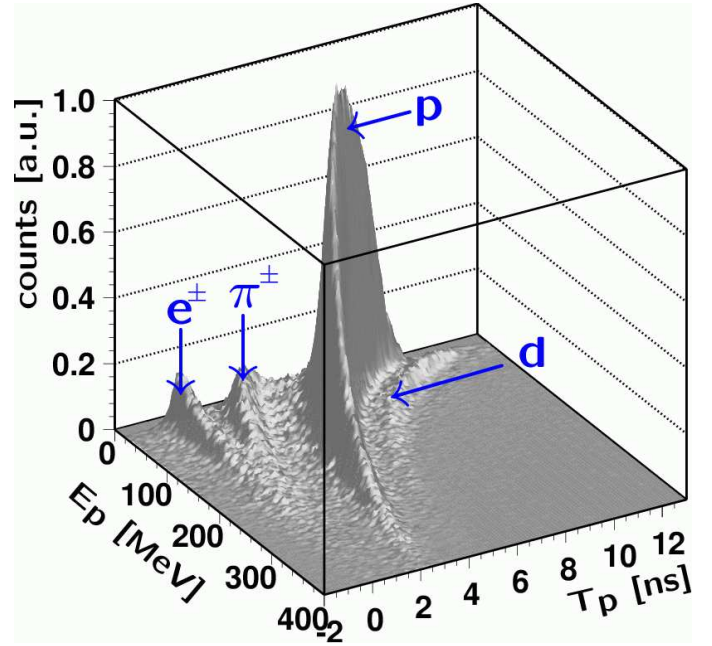


Fig. 5. Time-of-flight versus energy. The upper part shows a three-dimensional representation of the TOF-versus-E spectrum. The bands for electrons, charged pions, protons, and even deuterons are clearly visible. The bottom part shows a projection. Left hand side: data, right hand side MC simulation for the $\pi^0\pi^\pm$ reaction (only the charged pions were tracked by GEANT). The lines indicate the applied cuts.

sus energy analysis. The corresponding distributions of deposited energy E_p versus time-of-flight T_p are summarized in fig. 5. They are compared to the results of an MC simulation of $\pi^0\pi^\pm$ production. The shape of the pion bands in the data and the simulation are in good agreement. It should be noted, that π^+ and π^- behave identically in the TOF-versus-E spectra. This is not trivial since the π^- get absorbed by nuclei once they have deposited their kinetic energy, while the π^+ decay via the chain $\pi^+ \rightarrow \mu^+\nu_\mu \rightarrow e^+\nu_e\nu_\mu$ after they have been stopped. However, the kinetic energy of the decay muons is small and their lifetime (2.2×10^{-6} s) is much longer than the electronic gates so that the energy deposition from the decay positrons is not measured. In the MC simulations particles were only tracked for times corresponding to the hardware gate lengths used in the experiment. Since the time-of-flight is more precisely known than the deposited energy of the pions, their kinetic energies were

re-calculated from the time-of-flight. The region accepted for pion candidates in TOF-versus-E is indicated in fig. 5. In order to suppress background from $\eta \rightarrow \pi^0\pi^+\pi^-$ decays it was furthermore required in the event selection, that no second particle fulfilled the charged pion condition.

The pion band in the TOF-versus-E analysis is not background free (see fig. 5). There is some chance that protons leak into it. This happens for example for high energy protons which punch through the BaF_2 modules and thus deposit too little energy or for protons that scatter on their way to the detector (e.g. in the target chamber). These misidentified protons are in particular a problem at low incident photon energies, where the cross section for the potential background final state $p\pi^0$ from single π^0 production via the Δ resonance is larger than the $\pi^0\pi^\pm$ cross section by more than an order of magnitude. A suppression of this background is only possible via the reaction kinematics. However, one must take into account that protons, which are misidentified as pions, are assigned wrong kinetic energies since the energies of charged particles are based on the time-of-flight measurement using the mass of the particle. Therefore, only constraints based on the kinematics of the π^0 mesons can be used. At very forward angles this background was so large that the forward wall of the detector setup was not used for the charged pion analysis, which means that charged pions were only identified for laboratory polar angles larger than 22° .

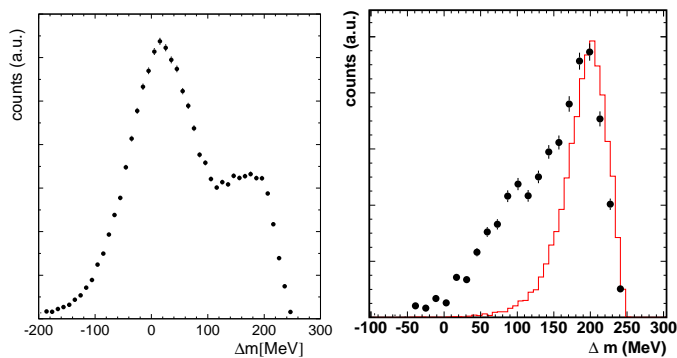


Fig. 6. Missing mass spectrum of $\pi^0\pi^+$ events for the background hypothesis $p\pi^0$ ($E_\gamma = 400 - 460$ MeV).

The most efficient method for the identification of single π^0 photoproduction is again the missing mass Δm calculated under the assumption of a quasi-free reaction mechanism (analogous to eq. 2 with the sums running only over the two decay photons). The result of this analysis for the critical low energy region is shown in fig. 6. The plot on the left hand side shows the missing mass for the hypothesis of single π^0 production for events where only the detection of a neutral pion was required. It shows a clear peak around zero corresponding to single π^0 production and the contribution from multiple pion production at larger missing masses. The right hand side shows the spectrum under the condition that an additional particle was detected which fulfills the pion TOF-versus-E condition. The data are compared to a MC simulation of the

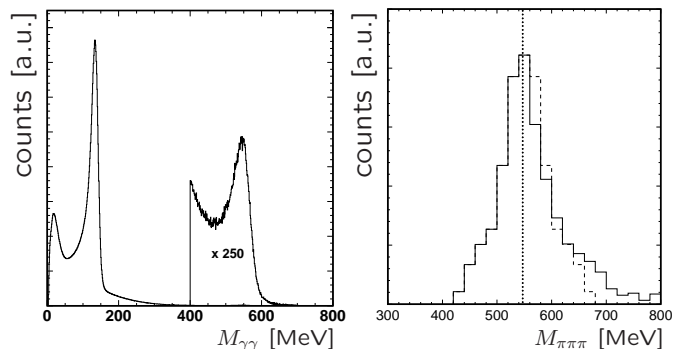


Fig. 7. Left hand side: invariant mass spectrum of photon pairs. Right hand side: invariant mass spectrum of $\pi^0\pi^\pm\pi^\pm$ events. The dotted line indicates the nominal position of the η peak. The dashed histogram is the mirror image of the left hand side of the peak (see text).

$\pi^0\pi^\pm$ final state. Some residual background from misidentified protons is visible at missing masses lower than 150 MeV. For further analysis only events with a single π^0 missing mass above 150 MeV were accepted.

Finally, the photoproduction of η mesons was analyzed for the two decay modes $\eta \rightarrow \gamma\gamma$ and $\eta \rightarrow \pi^0\pi^+\pi^-$. Since the cross section for the $^{40}\text{Ca}(\gamma, \eta)X$ reaction is known from previous experiments [47], this reaction can be used to estimate systematic effects in the detection of photons and charged pions and thus it helps to approximate the systematic uncertainties of the double pion production cross sections. The $\eta \rightarrow \gamma\gamma$ decay channel was identified with a standard invariant mass analysis of photon pairs (see fig. 7, left hand side). Events with invariant masses between 500 MeV and 600 MeV were selected. This is the range where the invariant mass peak is practically free of background, which has been investigated in detail for previous η production experiments with TAPS at MAMI at incident photon energies below 800 MeV ([47, 48, 49, 50]). For the analysis of the $\eta \rightarrow \pi^0\pi^+\pi^-$ decay in a first step $\pi^0\pi^\pm$ pairs were selected with the same cuts as for double pion production. In a second step a further hit fulfilling the TOF-versus-E condition for charged pions was required and finally the invariant mass of the three pions was constructed (see fig. 7, right hand side). The spectrum is dominated by the invariant mass peak of the η -meson, however there is also a small contribution from $\pi^0\pi^\pm\pi^\pm$ final states not related to η decays. Since the sum of the mass of the three pions sets a low mass limit and the total available energy a high mass limit of the distribution, the background populates similar invariant masses as the η decays and cannot be efficiently suppressed by a cut on invariant mass. For further analysis all entries in the invariant mass spectrum have been accepted, but the resulting cross section has been corrected for the obvious background contribution at large invariant masses. For this correction the left hand side of the peak was mirrored around the peak position (dashed histogram) and the access on the right hand side above this mirror image was assigned to the background. This procedure results

most likely in a slight underestimation of the total background.

4 Determination of cross sections

The absolute normalization of the cross sections was obtained (see ref. [34] for details) from the target density ($(1.52 \pm 0.01) \text{ g/cm}^2$), the photon flux, the decay branching ratio of $\pi^0 \rightarrow \gamma\gamma$, and the acceptance and detection efficiency of the TAPS detector. The latter was obtained from MC simulations with the GEANT3 package [46]. For the simulations the pion pairs have been generated according to phase space distributions in quasifree kinematics taking into account the Fermi motion of the nucleons. FSI was taken into account as in [41] in a simple approximation, where pions scatter randomly off nucleons according to their mean-free path. It was then checked, that missing mass-, kinetic energy-, and angular distributions were in agreement with the simulations.

For the extraction of the η photoproduction cross section from the $\eta \rightarrow \gamma\gamma$ decay the detection efficiency was obtained from MC simulations as function of laboratory angle and energy of the mesons as in [47]. This means that it becomes independent on assumptions about energy or angular distributions of the mesons. This is not possible for the $\eta \rightarrow \pi^0\pi^+\pi^-$ channel since the analysis used cuts on the reaction kinematic which depend on the incident photon energy. However, in this case the cross sections extracted from the $\eta \rightarrow \gamma\gamma$ channel can be used as input for the event generator. This is possible since the relatively long-lived η mesons decay always outside the nucleus so that the decay pions are not influenced by additional FSI effects. The results for the total cross section of η production are summarized in fig. 8. The agreement between the previous data from [47] and the present results is quite good for both decay channels and can be used to estimate the systematic uncertainties.

5 Systematic uncertainties

The systematic uncertainties for the two reaction channels and for different energy ranges arise from different sources, which are briefly discussed in this section.

We start with double π^0 photoproduction below the η production threshold (i.e. for $E_\gamma \leq 550 \text{ MeV}$). The identification of photons in the TAPS detector is very clean (see e.g. ref. [50]), and the suppression of background by the invariant mass analysis (see fig. 3) is efficient. As shown in fig. 4 (left hand side), no background is visible in the missing mass spectrum for incident photon energies below 500 MeV, and the shape of the missing mass spectrum is excellently reproduced by the Monte Carlo simulation. The missing mass cut is therefore irrelevant in this energy region. Furthermore, in a previous experiment [9], with an earlier stage of the TAPS detector, the reaction was investigated below the η threshold from an analysis of events with three photons. In this case, only identification of one

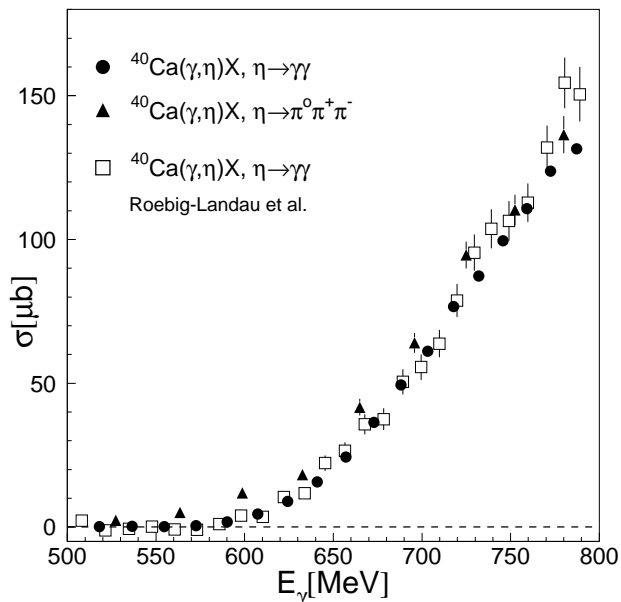


Fig. 8. Total cross sections for η photoproduction off calcium. Compared are the results for the $\eta \rightarrow \gamma\gamma$ and $\eta \rightarrow \pi^0\pi^+\pi^-$ decays to the results from a previous measurement [47].

π^0 meson and an additional photon was required. Such an analysis was possible since the only physical background in this energy range comes from the reaction $\gamma N \rightarrow \gamma'\pi^0 N$. Compared to double π^0 production, the cross section of this background reaction is smaller by more than an order of magnitude [51], and the contribution to the three-photon sample was suppressed by another order of magnitude relative to the $\pi^0\pi^0$ channel via detection efficiency (three-out-of-three versus three-out-of-four detected photons). The result of this analysis for the total cross section is compared in fig. 9 to the present result. The systematic difference between the two excitation functions is only 3 %, although the detector geometry, the cuts for the reaction identification, and the detection efficiencies were very different. We therefore estimate the systematic uncertainty of the double π^0 data below the η -threshold with 5 %.

At higher incident photon energies two effects increase the systematic uncertainty for the double π^0 channel. Background from $\eta \rightarrow 3\pi^0$ decays, where the decay photons from one pion escape detection, becomes important. At the same time, the probability of re-scattering of the pions from the double π^0 production in the nucleus increases, since the mean free path of pions decreases strongly with increasing kinetic energy [9]. Together with the smearing of the reaction kinematics due to Fermi motion, the re-scattering results in a significant fraction of events which in the missing mass analysis overlap with the η background (see fig. 4). In the analysis, only events with missing masses between 100 and -100 MeV were accepted for double π^0 production. The fraction of true $2\pi^0$ events, which do not pass this cut, was determined from the Monte Carlo simulations and corrected. The background from η events which pass this cut can be subtracted, since the η

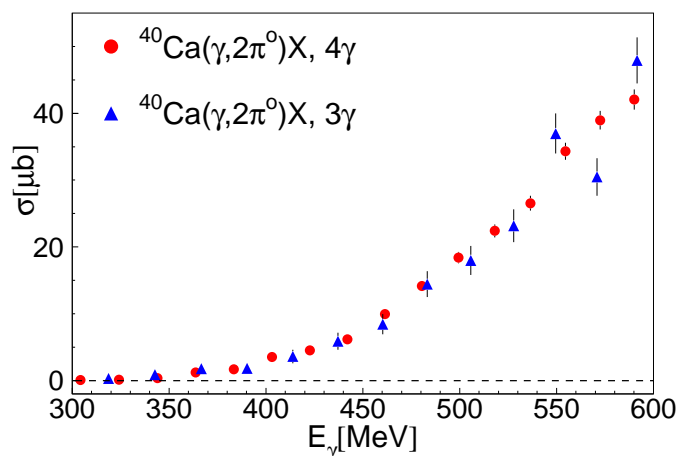


Fig. 9. Total cross sections for double π^0 production extracted from events with three [9] and four detected photons.

cross section is precisely known from the $\eta \rightarrow \gamma\gamma$ decay channel. This, however, involves a Monte Carlo simulation of $\eta \rightarrow 3\pi^0$ events. Both simulations contribute to the systematic uncertainty. Among these two, the $2\pi^0$ simulation is more critical since it involves model assumptions about the pion FSI. From a variation of the missing mass cut we estimate the uncertainty at the 10 % level for the highest incident photon energies. Therefore a linearly rising systematic error (0 % at 550 MeV, 10 % at 800 MeV) is added in quadrature.

The systematic uncertainty for the mixed charge channel is larger since for the charged pion we do not have the efficient invariant mass filter. A check of the simulated detection efficiency for charged pions is obtained from the analysis of the $\eta \rightarrow \pi^0\pi^+\pi^-$ decay, where it enters squared. The agreement between the cross sections from the two different η decays (see fig. 8) limits the systematic uncertainty for detection of a $\pi^0\pi^\pm$ pair to the 15 % range. At low incident photon energies the main source for systematic uncertainties is background due to misidentification of recoil protons from single π^0 production as charged pions (see sec. 4), which is suppressed by a missing mass cut (see fig. 6). Also from the comparison of the simulated missing mass spectrum to the measured distribution, a 15 % uncertainty at the lowest incident photon energies appears realistic. It should be noted that the fraction of true double pion events, which do not pass the 150 MeV cut, enters of course via the Monte Carlo simulations into the detection efficiency. Systematic effects therefore arise only from the correct representation of the double pion reaction in the simulation and from residual proton background, which is not eliminated by the cut. The relative importance of the proton background decreases with increasing incident photon energy since the cross section ratio of single π^0 to $\pi^0\pi^\pm$ production drops by more than an order of magnitude between 450 and 600 MeV, although at the same time the kinematic separation of the background gets worse due to pion re-scattering.

The relative contribution of background from η -decays ($\eta \rightarrow \pi^0\pi^+\pi^-$) is smaller by roughly an order of magni-

tude compared to the neutral channel. This is a combined effect of cross section ratios, η decay branching ratios and misidentification probability (π^0 and one of the charged pions must be detected while any pair out of three π^0 's is possible). Therefore it was not attempted to suppress this background with further cuts, but the simulated contribution was subtracted from the cross section. The related systematic uncertainty rises from threshold to high incident photon energies to a few per cent and counteracts the dropping of the uncertainty related to the above discussed background from single π^0 production. In addition, at higher incident photon energies a small contamination from $\pi^0\pi^\pm\pi^\pm$ events not originating from η decays may contribute (few per cent level, see fig. 7). We have thus assumed a conservative total uncertainty of 15 % for all incident photon energies.

Finally, an overall normalization uncertainty for the luminosity (target surface thickness and photon flux) of 2 - 3 % must be added.

6 Results

The total cross sections for the two double pion production channels are compared in fig. 10 to data off the nucleon. Two remarks must be made. The unpolarized double pion data off the nucleon measured with DAPHNE at MAMI [27,28] was recently revised [32]. The data shown for the $n(\gamma, \pi^0\pi^-)p$ reaction are the result of this re-analysis [29]. The total cross section for $\pi^0\pi^\pm$ production off ^{40}Ca from the TAPS experiment reported in [9] is slightly higher than the present result (approximately 10 % at 800 MeV). This discrepancy is due to the background from protons leaking into the pion TOF-versus-E band, which was not efficiently enough suppressed in the earlier analysis.

When properly scaled by the mass number dependence (as discussed in detail in [9,10]) the total cross section for the $\pi^0\pi^0$ channel is in excellent agreement with the deuteron data over the full energy range, indicating that only trivial effects like FSI influence the nuclear cross section. The situation is less clear for the $\pi^0\pi^\pm$ reaction. The nuclear data show a smooth behavior very similar to the $n(\gamma, \pi^0\pi^-)p$ reaction, while the $p(\gamma, \pi^0\pi^+)n$ excitation function has a pronounced peak in the second resonance region. This behavior might contribute to the still not understood complete suppression of the second resonance bump in total photoabsorption data [52]. At least for this channel, a part of the effect might be due to a difference in proton and neutron cross section. However, since the $\pi^0\pi^+$ cross section is measured off the free proton and the $\pi^0\pi^-$ cross section off the neutron bound in the deuteron a more detailed investigation of possible nuclear effects in the deuteron is highly desirable.

The main motivation for this experiment was the investigation of the $\pi - \pi$ invariant mass distributions in view of possible in-medium modifications of the strength in the scalar, iso-scalar channel. For two reasons low incident photon energies are advantageous for this analysis. First this avoids the additional background from triple

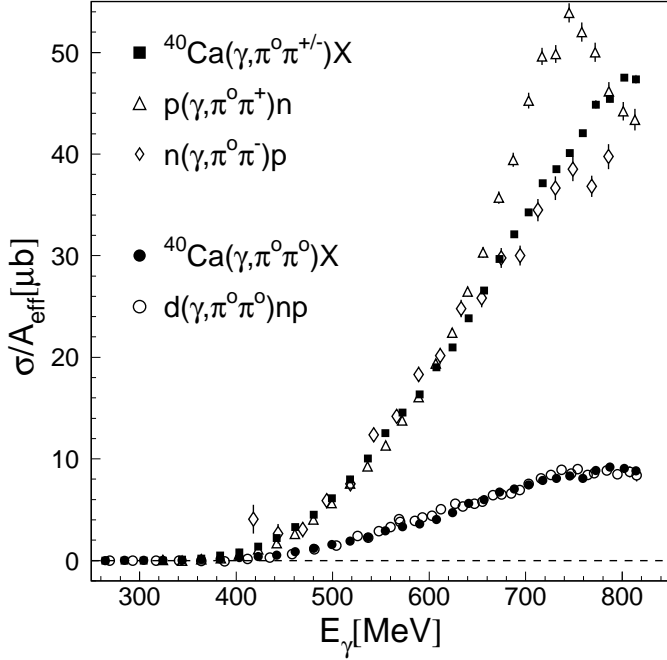


Fig. 10. Total cross sections for $\pi^0\pi^0$ and $\pi^0\pi^\pm$ photoproduction off ^{40}Ca compared to $d(\gamma, \pi^0\pi^0)np$ [36] respectively to $p(\gamma, \pi^0\pi^+)n$ [37] and $n(\gamma, \pi^0\pi^-)p$ [28, 29]. Cross sections are normalized to $A_{eff} = A^{2/3}$ for calcium and $A_{eff} = A$ for $A = 1, 2$.

pion decays of the η meson, which would give rise to additional systematic uncertainties. Furthermore, at low incident photon energies the kinetic energies of the produced pions are small. This is advantageous because low energy pions, which have only a small chance to excite the nucleon to the Δ resonance, are much less affected by FSI [9]. On the other hand, the cross section drops strongly towards the production thresholds, so that some compromise is necessary.

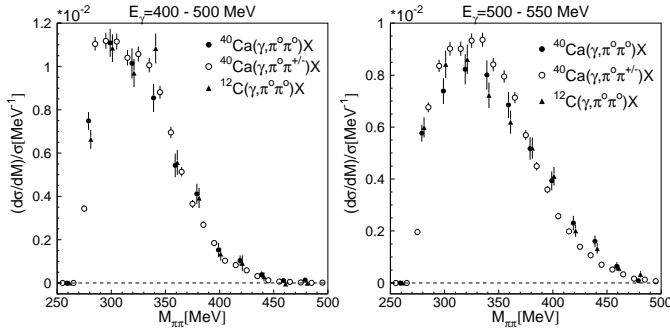


Fig. 11. Pion-pion invariant mass distributions for two different ranges of the incident photon energy normalized to the total cross section. The distributions from ^{40}Ca for $\pi^0\pi^0$ and $\pi^0\pi^\pm$ are compared to each other and to the $\pi^0\pi^0$ distributions from ^{12}C [41].

The measured distributions for two ranges of incident photon energies (400 MeV- 500 MeV and 500 MeV -550

MeV) are summarized in fig. 11 and compared to previous results for carbon [41]. The distributions for the two different charge channels and also for the two different nuclei are very similar. For ^{40}Ca we do not observe such an important shift of the $\pi^0\pi^0$ invariant mass distributions towards small invariant masses as has been found for lead [41], neither relative to the $\pi^0\pi^\pm$ channel for Ca nor in the comparison to $\pi^0\pi^0$ off carbon nuclei.

For a more detailed comparison the cross section ratios $C_{\pi\pi}(Ca/C)$ and $C_{\pi\pi}(\pi^0\pi^0/\pi^0\pi^\pm)$ defined by:

$$C_{\pi\pi}(Ca/C) = \frac{d\sigma_{Ca}(\pi^0\pi^0)}{\sigma_{Ca}(\pi^0\pi^0)dM} \bigg/ \frac{d\sigma_C(\pi^0\pi^0)}{\sigma_C(\pi^0\pi^0)dM} \quad (3)$$

$$C_{\pi\pi}(\pi^0\pi^0/\pi^0\pi^\pm) = \frac{d\sigma_{Ca}(\pi^0\pi^0)}{\sigma_{Ca}(\pi^0\pi^0)dM} \bigg/ \frac{d\sigma_{Ca}(\pi^0\pi^\pm)}{\sigma_{Ca}(\pi^0\pi^\pm)dM} \quad (4)$$

where $\sigma_X(\pi^0\pi^c)$, X =carbon, calcium are the total cross sections and $d\sigma/dM$ the invariant mass distributions, are shown in fig. 12. In line with the previous results for carbon and lead [41] some low mass enhancement of the $\pi^0\pi^0$ final state versus the $\pi^0\pi^\pm$ final state is also visible for calcium. However, there is no significant difference between the $\pi^0\pi^0$ distributions off carbon and off calcium. This means that the size of possible in-medium effects is comparable for carbon and calcium, while significantly stronger effects had been found for lead [41].

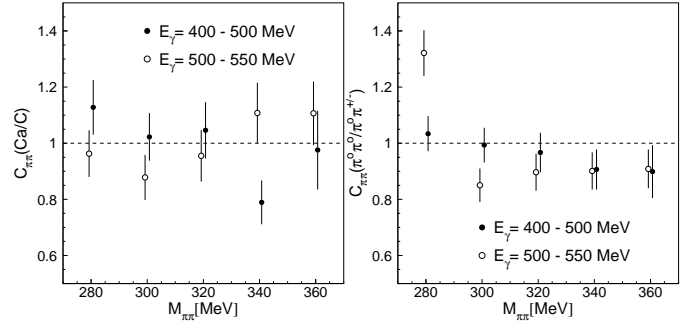


Fig. 12. Cross section ratios $C_{\pi\pi}(Ca/C)$ and $C_{\pi\pi}(\pi^0\pi^0/\pi^0\pi^\pm)$ for low invariant masses.

7 Comparison to results of the BUU-model

The quantitative discussion of the experimental results requires a detailed understanding of the ‘trivial’ in-medium effects like the smearing of cross sections due to the momentum distributions of the bound nucleons, collisional broadening of nucleon resonances due to additional decay channels like $NN^* \rightarrow NN$, Pauli-blocking of final states, and final state interactions of the pions. These effects have been intensively studied in the framework of coupled channel transport models based on the semi-classical Boltzmann-Uehling-Uhlenbeck (BUU) equation (see [53, 54, 55] for details of the model). Recently Mühlich et al. [56] and Buss et al. [57] have performed detailed calculations of the nuclear double pion photoproduction reactions

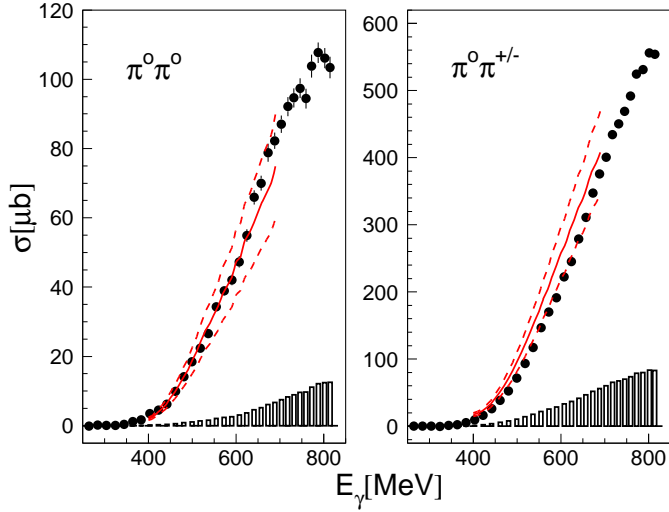


Fig. 13. Total cross sections compared to results of the BUU model [57]. The bars at the bottom represent the systematic uncertainty of the data (see sec. 5), the dashed lines represent the error band for the BUU calculation.

in the framework of this model. In the latter work, special emphasis was laid on the description of the scattering and absorption properties of low energy pions.

Apart from the inherent assumptions and approximations made in semi-classical transport models, systematic uncertainties of the calculations arise from the uncertainty of the cross sections of the elementary production reactions and the uncertainty of the cross sections involved in the description of pion FSI. Some indication for the correct treatment of pion FSI comes from a comparison [58] of model calculations and experimental results for pion-induced double charge exchange reactions, which are very sensitive to details of pion FSI. It is thus assumed, that the major uncertainty is related to the experimentally determined elementary production cross sections of pion pairs off nucleons. Buss and co-workers [57] estimate a systematic 20 % uncertainty of their results for the $\pi^0\pi^0$ channel from a simultaneous variation of all input cross sections to their $\pm 1\sigma$ limits. This estimate is conservative since no cancellation of systematic errors from different reaction channels is considered. The largest uncertainty is related to the $\gamma n \rightarrow n\pi^0\pi^0$ channel. The uncertainty estimated in [57] for the $\pi^0\pi^\pm$ final state is much smaller, however this was based only on the statistical uncertainties of the input data and has neglected the systematic ones, which are also typically on the 10 - 15 % level. Therefore we assume also for this channel a 15 % systematic uncertainty. These model uncertainties and also the systematic uncertainties of the data are indicated in figs. 13,14 as dashed lines, respectively bar charts.

The overall agreement between the model results and the data for the total cross sections is good within the systematic uncertainties (see fig. 13), it is excellent for the $\pi^0\pi^0$ channel in the energy range of interest for the invariant mass distributions. Up to now, reliable BUU calculations are not available for incident photon energies above 700 MeV, since in this region the elementary free nucleon

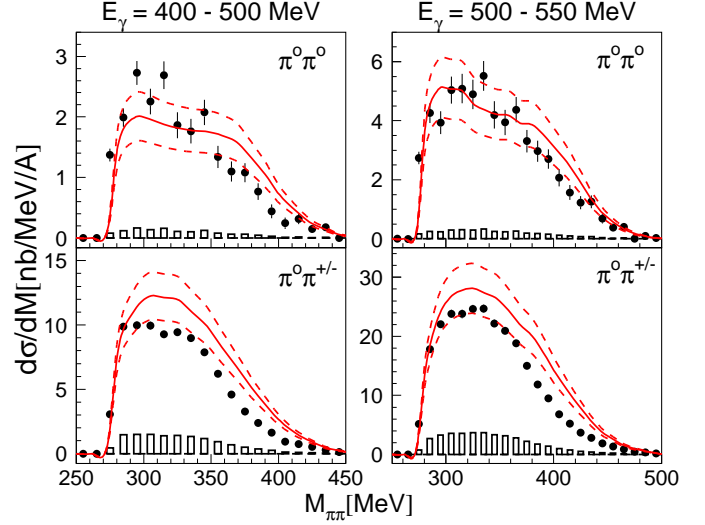


Fig. 14. Pion-pion invariant mass distributions compared to results of the BUU model [57]. The bars at the bottom represent the systematic uncertainty of the data (see sec. 5), the dashed lines represent the error band for the BUU calculation.

cross sections have too large uncertainties for some channels.

An important result of this model calculations is, that even without any explicit in-medium modification of the $\pi^0\pi^0$ channel, the respective invariant mass distributions show a significant softening for heavy nuclei [57]. In the model, this effect arises solely from FSI of the pions. Part of it comes from the fact that the πN absorption cross section increases strongly with pion kinetic energy, so that pions with larger kinetic energies are more strongly depleted via the $\pi N \rightarrow \Delta$, $\Delta N \rightarrow NN$ reaction path. But not only the absorptive part of the FSI is important, also important are re-scattering processes which tend to decrease the pion kinetic energy and thus the average pion - pion invariant masses. This effect is enhanced due to charge exchange scattering, which mixes the contributions from the different charge channels. Since the total cross section for $\pi^0\pi^\pm$ production is much larger than the $\pi^0\pi^0$ cross section, the latter receives significant side feeding from the mixed charge channel via $\pi^\pm N \rightarrow N\pi^0$ scattering, which increases the fraction of re-scattered low-energy pions in this channel. In the same way, re-scattering of $\pi^+\pi^-$ contributes to the $\pi^0\pi^\pm$ channel. This result means, that the relative softening of the $\pi^0\pi^0$ invariant mass by itself is no evidence for an in-medium modification of the pion - pion interaction, but the argument becomes quantitative, requiring a comparison of the experimental results to calculations which account for the trivial FSI effects.

The invariant mass distributions for the two energy ranges are compared to the BUU results in fig. 14. The general tendency of a softening of the distributions is reproduced by the calculations as a consequence of FSI effects. On a quantitative level, the data for the $\pi^0\pi^0$ invariant masses for the lowest incident photon energies seem to be slightly stronger downward shifted than predicted. One should note that this effect cannot be completely ex-

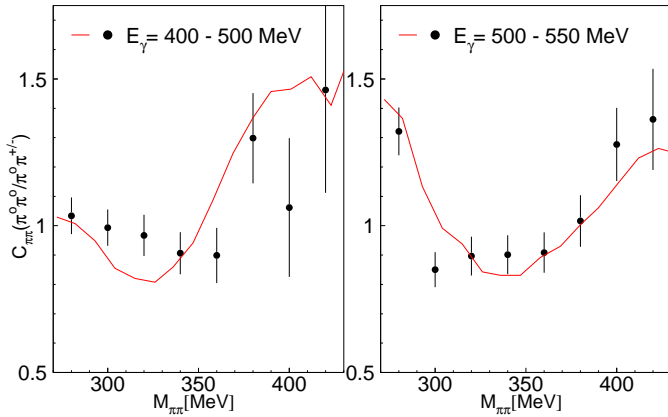


Fig. 15. Cross section ratio $C_{\pi\pi}(\pi^0\pi^0/\pi^0\pi^\pm)$ compared to the results of the BUU model [57]. Symbols: data, curves BUU results [57]. Left hand side: incident photon energies 400 - 500 MeV, right hand side: incident photon energies 500 - 550 MeV.

plained by the systematic uncertainties of data and model results, since the uncertainties are not strongly invariant mass dependent but rather related to the absolute scale of the cross section. The cross section for the mixed charge channel is somewhat overestimated by the model, in particular for large invariant masses. This absolute normalization cancels in the $C_{\pi\pi}(\pi^0\pi^0/\pi^0\pi^\pm)$ ratio, which is compared to the BUU results in fig 15. Within the statistical uncertainties, the agreement between data and model results is good. This means that the relative shapes of the $\pi^0\pi^0$ and $\pi^0\pi^\pm$ invariant mass distributions can be almost completely reproduced from FSI effects.

8 Summary and conclusions

Total cross sections and pion-pion invariant mass distributions have been measured for $\pi^0\pi^0$ and $\pi^0\pi^\pm$ photoproduction off ^{40}Ca nuclei. When scaled by $A^{2/3}$ the total cross sections agree quite well with the average of the elementary cross sections off the proton and the neutron. The only exception is the mixed charge final state in the second resonance region, where the reaction off the free proton shows a more pronounced signal for the resonance bump.

The invariant mass spectra show a similar effect as already reported in [41] for carbon and lead nuclei, namely a softening of the $\pi^0\pi^0$ distributions relative to the $\pi^0\pi^\pm$ distributions. The strength of the effect is comparable to carbon.

The data have been compared to calculations in the framework of the BUU model [57]. A sizable part of the in-medium effects can be explained by the model by final state interaction effects, which tend to shift re-scattered pions to smaller kinetic energies. Only for the lowest incident photon energies a small additional downward shift of the strength to small invariant masses for the $\pi^0\pi^0$ channel may be visible.

9 Acknowledgments

We wish to acknowledge the excellent support of the accelerator group of MAMI, as well as many other scientists and technicians of the Institut für Kernphysik at the University of Mainz. We thank O. Buss, U. Mosel, and P. Mühlich for many valuable discussions and the communication of the BUU results. This work was supported by Schweizerischer Nationalfonds, Deutsche Forschungsgemeinschaft, and the UK Engineering and Physical Sciences Research Council.

References

1. M. Lutz, S. Klimt, and W. Weise, Nucl. Phys. **A542** (1992) 521.
2. G. Agakichiev et al., Phys. Rev. Lett. **75** (1995) 1272.
3. D. Adamova et al., Phys. Rev. Lett. **91** (2003) 042301.
4. S. Damjanovic et al., Nucl. Phys. **A774** (2006) 715.
5. M. Naruki et al., Phys. Rev. Lett. **96** (2006) 092301.
6. D. Trnka et al., Phys. Rev. Lett. **94** (2005) 192303.
7. M. Post, S. Leupold, and U. Mosel, Nucl. Phys. **A741** (2004) 81.
8. B. Krusche et al., Phys. Rev. Lett. **86** (2001) 4764.
9. B. Krusche et al., Eur. Phys. J. **A22** (2004) 277.
10. B. Krusche et al., Eur. Phys. J. **A22** (2004) 347.
11. B. Krusche, Prog. Part. Nucl. Phys. **55** (2005) 46.
12. J. Lehr and U. Mosel, Phys. Rev. **C64** (2001) 042202.
13. V. Bernard, U.-G. Meißner, and I. Zahed, Phys. Rev. Lett. **59** (1987) 966.
14. W.-M. Yao et al., J. Phys. **G33** (2006) 1.
15. I. Caprini, G. Colangelo, and H. Leutwyler, Phys. Rev. Lett. **96** (2006) 132001.
16. T. Hatsuda, T. Kunihiro, and H. Shimizu, Phys. Rev. Lett. **82** (1999) 2840.
17. Z. Aouissat, G. Chanfray, P. Schuck, and J. Wambach, Phys. Rev. **C61** (2000) 012201.
18. H.C. Chiang et al., Nucl. Phys. **A644** (1998) 77.
19. L. Roca, E. Oset, and M.J. Vicente Vacas, Phys. Lett. **B541** (2002) 77.
20. G. Chanfray et al., Eur. Phys. J. **A27** (2006) 191.
21. F. Bonutti et al., Phys. Rev. Lett. **77** (1996) 603.
22. F. Bonutti et al., Phys. Rev. **C 60** (1999) 018201.
23. F. Bonutti et al., Nucl. Phys. **A 677** (2000) 213.
24. P. Camerini et al., Nucl. Phys. **A735** (2004) 89.
25. N. Grión et al., Nucl. Phys. **A763** (2005) 80.
26. A. Starostin et al., Phys. Rev. Lett. **85** (2000) 5539.
27. A. Braghieri et al., Phys. Lett. **B363** 1995 46.
28. A. Zabrodin et al., Phys. Rev. **C55** (1997) R1617.
29. P. Pedroni, private communication.
30. A. Zabrodin et al., Phys. Rev. **C60** (1999) 055201.
31. J. Ahrens et al., Phys. Lett. **B551** (2003) 49.
32. J. Ahrens et al., Phys. Lett. **624** (2005) 173.
33. F. Härter et al., Phys. Lett. **B401** (1997) 229.
34. B. Krusche et al., Eur. Phys. J. **A6** (1999) 309.
35. M. Wolf et al., Eur. Phys. J. **A9** (2000) 5.
36. V. Kleber et al., Eur. Phys. J. **A9** (2000) 1.
37. W. Langgärtner et al., Phys. Rev. Lett. **87** (2001) 052001.
38. M. Kotulla et al., Phys. Lett. **B578** (2004) 63.
39. Y. Assafiri et al., Phys. Rev. Lett. **90** (2003) 222001.
40. B. Krusche and S. Schadmand, Prog. Part. Nucl. Phys., **51** (2003) 399.

41. J.G. Messchendorp et al., Phys. Rev. Lett. **89** (2002) 222302, and S. Schadmand priv. com.
42. I. Anthony et al., NIM **A301** (1991) 230.
43. Th. Walcher, Prog. Part. Nucl. Phys. **24** (1990) 189.
44. R. Novotny, IEEE Trans. on Nucl. Science **38** (1991) 379.
45. A.R. Gabler et al., Nucl. Instr. and Meth. **A346** (1994) 168.
46. R. Brun et al., GEANT, Cern/DD/ee/84-1, 1986
47. M. Röbig-Landau et al., Phys. Lett. **B373** (1996) 45.
48. B. Krusche et al., Phys. Rev. Lett. **74** (1995) 3736.
49. B. Krusche et al., Phys. Lett. **B358** (1995) 40.
50. B. Krusche et al., Z. Phys. **A351** (1995) 237.
51. M. Kotulla et al., Phys. Rev. Lett. **89** (2002) 272001.
52. N. Bianchi et al., Phys. Lett. **B325** (1994) 249.
53. M. Effenberger et al., Nucl. Phys. **A614** (1997) 501.
54. S. Teiss et al., Z. Phys. **A356** (1997) 421.
55. P. Mühlich et al., Phys. Rev. **C67** (2003) 024605.
56. P. Mühlich et al., Phys. Lett. **B595** (2004) 216.
57. O. Buss, L. Alvarez-Ruso, P. Mühlich, U. Mosel, Eur. Phys. J. **A29** (2006) 189, and O. Buss, private communication.
58. O. Buss, L. Alvarez-Ruso, A.B. Larinov, U. Mosel, Phys. Rev. **C74** (2006) 044610.